Solubility of Pt and Rh in basalt-rhyolite mixtures: Implications for PGE saturation during crustal contamination

Victoria McKenzie

University of Toronto

2008

Supervisor: James Brenan

Abstract

The solubility of Pt and Rh as a function of silicate melt composition has been investigated. Pt/Rh_{10} alloy wire was homogenized with melt compositions systematically ranging between 100% natural basalt (from east Greenland) and 100% natural rhyolite (from Lake County Oregon), with 10, 30, 50, and 75% rhyolite in basalt compositions included. Experiments were performed at 1405 ± 3 °C, and $\log f O_2$ ~ -2.89 (FMQ buffer) for run durations between 5 and 100 hours. Samples were analyzed for trace concentrations using LA-ICP-MS, and major elemental concentrations using electron microprobe. A negative correlation was found between increasingly rhyolitic compositions and Pt and Rh solubility. Plots of Pt195 and Rh103 versus common oxides were generated, showing a second order dependence. A similar relationship was seen between the calculated compositional parameter, NBO/T, and Pt/Rh concentration. The degree of SiO_2 polymerization is proposed as the means for inhibiting dissolution of PGE in increasingly felsic melts. Rh was noted to show a greater solubility than Pt, and this may be due to less thermodynamic and structural barriers for Rh to overcome when forming an oxide. A model was proposed for the oversaturation of Pt and Rh during interdiffusion of rhyolite and basalt based on the difference between PGE solubility and concentration. This work could influence compositions used in further studies of PGE solubility, and also the enhance the understanding of PGE precipitation in chromatites.

Introduction

Platinum group elements (PGE: Pd, Pt, Ir, Os, Ru, and Rh) have undergone considerable study, as their anomalous abundance in the mantle has made them a focus for research in understanding Earth's early formation. The highly siderophile elements (HSE), of which the subset PGE belong, occur in approximately chondritic ratios in the mantle, suggesting that their presence results from the addition of a late chondritic veneer following the completion of core differentiation. Other models propose a continuous Earth accretion, wherein HSE were able to equilibrate at the base of a magma ocean where high temperatures and pressures decreased the typically high partition coefficients (Fortenfant *et. al.*, 2003; Ertel *et al.,* 1999; Holzheid *et al.,* 2000l; Borisov *et al.*, 1994). Investigating the behavior of these elements in a variety of systems could enhance understanding of Earth's terrestrial beginnings.

PGE are not only poorly understood in terms of their past role on Earth, but also their present role. The effect of mantle melting and the determination of whether PGE could be primary phases in mafic igneous systems have undergone some study. Strongly influenced by their high metal/silicate partition coefficients, some sources suggest that PGE tend to remain in residual sulfide during partial mantle melting (Ertel, *et al.*, 1999). Borisov and Palme (2000) studied a variety of noble metals and their solubilities in silicate melts. Platinum in particular was found to be influenced by the formation of alloys (Pt-Fe) which decreased solubility in silicate melts considerably. Though calculated to deplete Pt from partial melts, this effect was not actually observed in nature, suggesting mantle oxidizing conditions different to those studied experimentally. Cleary, the solubility behavior of PGE is a complex problem. As suggested by Fortenfant, *et al.* (2003), clarifying the problem

requires an understanding of the effects of oxygen fugacity, temperature, pressure, and silicate melt composition.

In general, the solubility of neutral metal atoms (M) in silicate melts relies on fO_2 by undergoing oxidation according to the reaction

$$M^{met} + (m/4)O_2 = MO^{sil}_{m/2}\,, \qquad (1)$$

where m is the valence state of the metal. To determine the equilibrium constant of this reaction (1), one can use

$$k = [(X_{MOm/2}{}^{*}\gamma_{MOm/2}]/[a_M{}^{*}\,(fO_2)^{m/4}], \qquad (2)$$

where X is mole fraction, a is activity, and γ is activity coefficient, with a= γ*X. Taking the log of both sides yields the expression,

$$\log k = \log[a_{MO^{m/2}}/a_M] - m/4\,\log(fO_2). \qquad (3)$$

Expression (3) can be made linear by considering a system of equilibrium between a pure metal and silicate melt, which has a metal activity of unity. Assuming the activity coefficient ($\gamma_{MOm/2}$) to be independent of fO_2, we can rearrange (3) into

$$\log X_{MOm/2} = \log k + m/4\,\log(fO_2) \qquad (4)$$

for a given T. The expression (4) yields a slope equal to m/4, where m is the oxidation state of the metal. Since k is a constant, the expression can be written in the more common form of

$$\log X_{MOm/2} = m/4 \log(fO_2) + \text{constant.} \quad (5)$$

The valence state of a metal can therefore be found experimentally by determining the relationship between log concentration and log (fO_2) (Borisov, Palme, & Spettel, 1994).

With the basis for fO_2 dependence established, several studies on the effects of oxygen fugacity on PGE solubility have been completed. Borisov and Palme (1997) conducted a study with fO_2 ranging from pure oxygen to 10^{-8} atm. Micronugget contamination resulted in unreliable data for fO_2 values $<10^{-5}$, but the at the highest oxygen fugacities, a negative correlation existed between increasing fO_2 and decreasing solubility, agreeing with the theoretical work.

In a similar study, Ertel *et al.* (1999) investigated Pt and Rh solubility at 1300°C ranging between oxygen fugacities 10^{-12} bar and 1 bar. Results showed steady increases and decreases at very high fO_2 values (pure air and Ar-O_2 mixtures), with concentrations of Pt and Rh decreasing with decreasing fO_2. Lower fO_2 ($fO_2 <10^{-5}$) conditions yielded heterogeneity in the samples which rendered the fO_2 – PGM solubility relationship difficult to asses. By using only the data from the higher fO_2 runs, the solubility constants were determined.

Problems relating to glass heterogeneity were observed beginning at intermediate oxygen fugacities ($\log fO_2$=-2.9), which is relevant to the methodology of this paper which intends to study solubility at the FMQ buffer. However, using laser ablation inductively-coupled mass spectrometry (LA-ICP-MS), Ertel *et al.* (1999) were able to bypass the anomalous values fairly easily, and the filtered values indicated similar behavior to the high

fO_2 data. The distribution coefficients were finally estimated to be $D_{Pt}^{met/sil} > 10^{11}$, and $D_{Rh}^{met/si} > 10^{9}$.

Another parameter which was found to have an impact on PGE solubility systems is temperature. Fortenfant *et al.* (2003) studied the temperature dependence of Pt and Rh solubility at the anorthite-diopside eutectic composition. A positive correlation was found between increasing temperature and the solubility of HSE in a siliceous melt. Experiments ranged from 1300°C to 1550°C, and between the upper and lower temperature limits, Rh concentration in the glasses nearly tripled, and Pt nearly doubled. The solubilities of Pt and Rh in a silicate melt as a function of fO_2 and temperature were expressed as

$$\log [Pt](ppm) = -3320(340)/T(K) + 2.0(0.2) + 0.5(2.5 + \log fO_2) \qquad (6)$$

$$\log[Rh](ppm) = -5440(450)/T(K) + 3.9\ (0.3) + 0.5(2.5 + \log fO_2), \qquad (7)$$

where both metals are assumed to be 2+ species.

Despite the positive correlation found between increasing temperature and solubility, the values of metal-silicate partition coefficients were found by extrapolation to be too high to support core-mantle equilibrium models. In addition, partition coefficients of Pt and Rh showed a difference of ~2 log units, which means that had core-mantle equilibrium been occurring, these elements would have differentiated too greatly to be present in the chondritic ratios now observed (Fortenfant, *et al.*, 2003).

Pressure is another important consideration in the core-mantle equilibrium models, which suggest equilibration occurring at the base of a magma ocean. To support this theory, the PGE partition coefficients would need to lower under high pressure conditions. Based

on the high-pressure silica solubility of moderately siderophile elements, Holzheid *et al.* (2000) tested the effect of high pressures (up to 16GPa) on Pt and Pd. It was determined that between the pressures of 0.5GPa and 16GPa, values did not show a trend suggesting correlation between increased pressure and decreased partition coefficients. The $D^{met/sil}$ of Pd was found to be in the order of 10^5 to 10^6, and Pt in the order of $>10^7$ to 10^9 for the aforementioned pressure range. The $D^{met/sil}$ would be expected to be ~1000 at the pressure and temperature at which metals and silicates equilibrate in order to support equilibrium partitioning at the base of a magma ocean. Again, the late chondritic veneer is suggested as a more likely explanation for the presence and distribution of HSEs in the mantle.

The final parameter worthy of study is composition. In addition to their study of fO_2 effects, Borisov and Palme (1997) studied the solubility of Pt at 2 compositions: the anorthite-diopside (AD) eutectic composition, and the $MgO*Al_2O_3*3SiO_2$ (MAS) system composotion. The MAS system was found to be about 2.5 times less soluble than the AD system. The compositions vary in silica content (MAS ~60% SiO_2, AD ~ 50% SiO_2), and therefore polymerizaton, with the MAS NBO/T ~ 1.3, and the AD NBO/T ~ 0.5.

Similar results were seen by Fargus, *et al.* (1999), who examined Pt solubility along the Ca-rich corner of the $CaO-Al_2O_3-SiO_2$ (CAS) ternary. Compositions with greater alumina content yielded greater Pt dissolution than those with high SiO_2 contents. The observations were explained by the unlikely structural correlation between SiO_2 and Pt, and the more predictable corner sharing arrangement between Pt^{6+} and Al^{4+} oxides. It is also suggested that dissolution may be enhanced by the addition of small alkali cations such as Na^+. Relevant network-modifying cations present in basaltic compositions are Fe^{2+} and Mg^{2+}, which likely cause changes in the polymerization of silicate melts (Walter & Thibault, 1995). In determining the partitioning behavior of tungsten and molybdenum, Walter and

Thibault (1995) concluded that compositional impacts on partition coefficients of HSEs cause variances of ~2 orders of magnitude, and therefore may be of greater importance than temperature in terms of PGE dissolution.

Compositional impacts on PGE solubility have not yet undergone methodical investigation, and the purpose of this study is to enrich the otherwise lacking data available on the topic. Systematic mixing of a natural rhyolite and basalt exposed to Pt-Rh_{10} alloy at fO_2 near the fayalite-magnetite- quartz (FMQ) buffer, as it is assumed to be in the upper mantle, will model the addition of crustal contamination to a Pt-Rh saturated basalt (Borisov & Palme, 2000). A compositional spectrum of 100% basalt to 100% rhyolite provides a gradient for the behavior of Pt, Rh, and other major and minor interacting elements. The incorporation of common crustal materials (silica, alumina) are expected to decrease the solubility of Pt and Rh in the melts.

Experimental Methods

Solubility measurements

Compositions employed in the solubility measurements, were a natural basalt and rhyolite (Table 1). The rhyolite is from Lake Country, Oregon and has a composition similar to the 0.2 GPa granite minimum (Best, 1982). The basalt, from east Greenland, is a microporphyritic alkali-olivine basalt, initially free of Pt and Rh (Hogg, 1985) (Table 1). The ground materials were calcined in alumina crucibles by heating from 500°C to 1000°C over 5 hours, then left at the upper temperature overnight. Samples were then air-cooled and stored in a dessicator.

Mixtures of 0%, 10%, 30%, 50%, and 75% rhyolite in basalt were weighed and ground using a mortal and pestle to homogenize. Wire loops were prepared using Pt-10%Rh alloy wire (0.020" width, or double-wound 0.010"), and ~100mg of dry sample were mixed with polyvinyl alcohol adhesive and pasted onto the loops (Figure 1).

Experiments using the pure rhyolite composition were done using fused rhyolite shards. The rhyolite was prepared by heating in an alumina crucible from 1000°C to 1400°C over 2hrs, and then left at 1400°C for 1 hour. The resulting glass was removed from the crucible and pieces of similar size to the beads were selected and wrapped in 0.010" alloy wire (Figure 1).

During experiments, wire loops of were suspended from a 4-pronged silica hook into a Deltech vertical tube gas-mixing furnace. An yttrium-doped zirconia oxygen probe was used to determine the fO_2 generated by CO_2 disproportionation within the furnace. The sensor generates an emf which can be equated to an fO_2 using the Nernst equation

$$EMF = (RT/nF) * \ln(fO_2/fO_{2\,ref}), \qquad (8)$$

in which R and F are the gas and Faraday constants, respectively, T is the absolute temperature, and $fO_{2\,ref}$=0.209 for air.

Table 1: Compositions of starting materials.

Oxide	Greenland Basalt (wt%) *	Lake County Obsidien (anhydrous) (wt%)**
SiO2	43.49	76.17(0.35)
TiO2	4.45	0.2(0.11)
Al2O3	6.82	13.76(0.2)
FeO*	14.11	1.36(0.17)
MnO	0.16	0.06(0.04)
MgO	14.81	0.27(0.03)
CaO	9.99	1.34(0.07)
Na2O	1.60	3.37(0.09)
K2O	1.18	3.65(0.09)
P2O5	0.54	0.07(0.04)
L.O.I	1.19	-

*XRF analysis, Hogg (1985)
**Electron microprobe analysis
LOI, loss on ignition; n.a., not analyzed

Figure 1: Photo a.) shows a typical assembly used to suspend samples in vertical tubee furnace. Photo b.) shows a peice of rhyolite glass used as an alternative to ground material, and wound with Pt/Rh alloy wire.

The measured emf was~185 ±6mV, corresponding to log$f$O$_2$~-2.89, or FMQ +3.8. Temperature was monitored using a type S thermocouple (PtRh$_{10}$/Pt), and held at 1405± 3°C. Experiments were plunged into the hot zone of the furnace and homogenized there for durations of 5, 10, 30, 50, 88 or 100hrs, with fO$_2$ requiring 10-15 minutes to achieve the desired value. Cold water was used to quench and terminate each time trial, and temperature and emf readings were taken before and after experimental runs (Table 2).

Table 2: Summary of experiments run at T=1678 +/-3 K and logfO2=-2.89.

		Starting Compositions	
Experiment ID	Run Duration (hr)	%Basalt	%Rhyolite
5R0	5	100	0
10R0	10	100	0
30R0	30	100	0
5R10	5	90	10
10R10	10	90	10
30R10	30	90	10
5R30	5	70	30
10R30	10	70	30
30R30	30	70	30
88R30	88	70	30
5R50	5	50	50
10R50	10	50	50
30R50	30	50	50
50R50	50	50	50
30R75	30	25	75
50R75	50	25	75
50R100	50	0	100
88R100	88	0	100
100R100	100	0	100

Analytical techniques

Trace Element Concentration Determination

Run products were mounted in epoxy and polished down to 1μm using alumina powder. Trace elements were determined by LA-ICP-MS at the University of Toronto Department of Geology. A frequency quintupled neodymium YAG laser operating at 213nm was employed in conjunction with a VG PQExcell quadrupole ICP-MS. Helium was used as a carrier gas through sample cell.

Analyses were collected in blocks of 20, with standard reference materials (NIST610 and JBsulfide) collected at the beginning and end of each. Typically 4-5 widely spaced analyses were done on each run-product glass. To eliminate surface contamination, the sample was subject to an initial pre-ablation pass, followed by at least 60 seconds of He flushing prior to data acquisition. Data acquisition involved 20 seconds of background collection with the laser off followed by 60 seconds of sample ablation. Table 3 shows the beam width, laser repetition rate, and output percentage used for standards and samples.

The NIST610 and samples were determined to contain significant amounts of ^{178}Hf and ^{179}Hf, requiring a correction for ^{178}Hf-^{16}O and ^{179}Hf-^{16}O interference with Pt of masses 194 and 195 respectively. Using data from a natural zircon analysis - with abundant Hf and no Pt - the ratios of hafnium oxide to hafnium were determined as ^{178}Hf-^{16}O/^{178}Hf = 0.001933 and ^{179}Hf-^{16}O/^{179}Hf = 0.002069. By multiplying the measured hafnium count by the ratio, and then subtracting this value from the appropriate Pt count, the oxide interference was eliminated. Data reduction was completed using GLITTER version

5.3 software. Data was integrated based on Pt values in order to avoid micronugget values from being incorporated into otherwise consistent data, which was generally found to be homogeneous (Figure 2). Ca and Cu determined from microprobe analysis were used as reference elements to correct ablation yields, but due to greater similarities in Pt^{194} and Pt^{195} concentrations, Cu-reduced data was used for further analysis. All trace element concentrations were averaged for each glass composition, and their standard deviations determined.

Major Element Concentration Determination

Major element concentrations in run-product phases were determined using a Cameca SX50 Electron Probe Microanalyser in the University of Toronto Department of Geology. The microprobe accelerating voltage was 15kV, the beam current 9.96nA, and the beam diameter was 10μm. Counting time of 20s was used for each element. The standards used were natural basalt glass (Si, Al, Fe, Mg), bustamite (Ca, Mg), sanidine (K), apatite (P), TiO_2 (Ti). Fifteen points on each sample were chosen for analysis. Raw counts were converted into concentrations using the ZAF algorithm. Analyses were rejected if oxide totals fell outside range of 98.5-101.5%. The average and standard deviation of elements for each composition were determined. Glass concentrations were found to be homogeneous, as the standard deviation of multiple analyses is similar to the precision from counting statistics.

Table 3: Laser conditions for LA-ICP-MS analyses.

	Laser Repetition Rate (Hz)	Beam width (micron)	Output (%)
NIST610	10	100	50-55
JB-sulfide	4	40	60
Run products	10	125	50-55

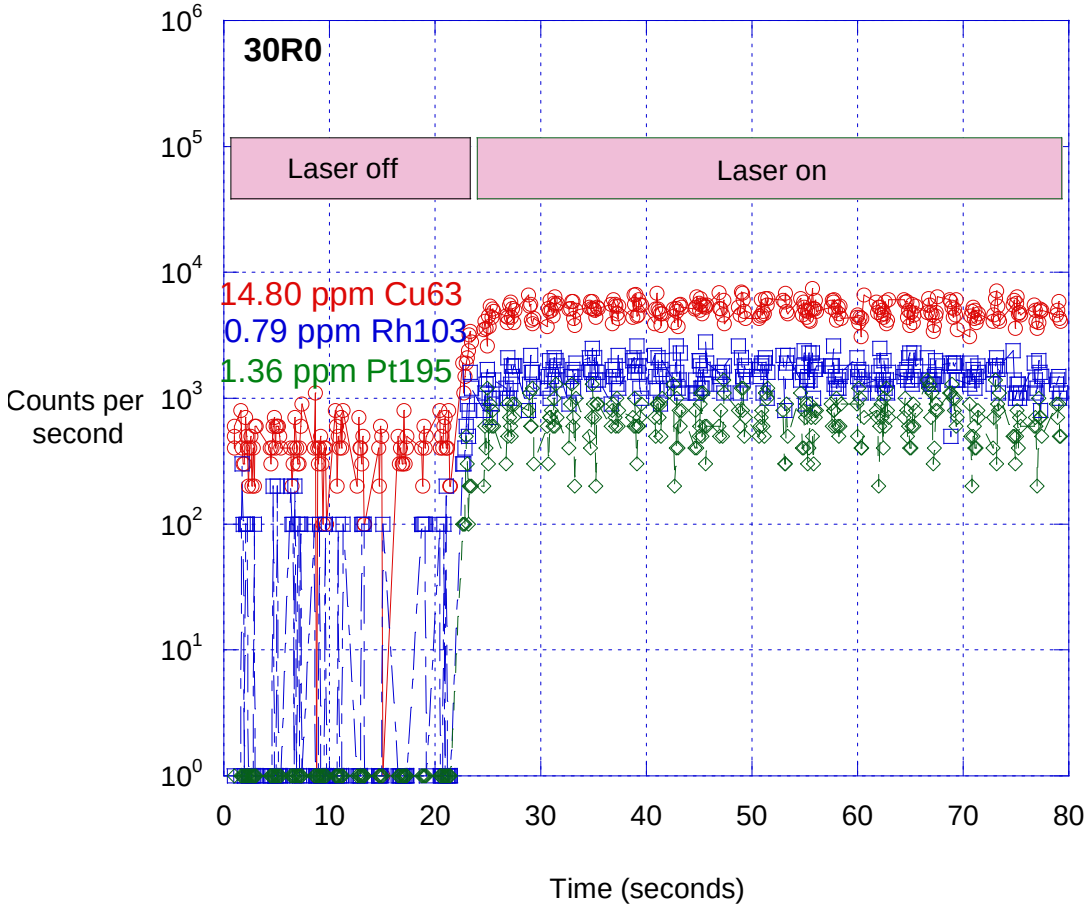

Figure 2: LA-ICP-MS time resolved data for Cu63, Rh103, Pt195 intensity spectra for a glass with 0% rhyolite, run for 30hrs. The glass is seen here to be homogeneous, but data underwent further intengration to eliminate small inhomogeneities. The first 20 seconds was background counting without ablation.

Table 4: Summary of trace element glass compositions determined by LA-ICP-MS

	Concentrations (ppm)					
Experiment ID	Rh103	Pt194	Pt195	Cu63	Cu65	Ni61
5R0	0.788(0.022)	0.855(0.014)	0.901(0.007)	67.77(0)	68.56(0.39)	390.46(20.43)
10R0	0.819(0.004)	0.861(0.013)	0.852(0.038)	32.36(0)	32.91(0.44)	370.12(6.86)
30R0	0.761(0.056)	0.821(0.014)	0.8195(0.07)	14.76(0)	15.06(0.79)	290.03(23.61)
5R10	0.613(0.028)	0.69(0.022)	0.693(0.025)	47.17(0)	47.84(0.32)	333.6(19.56)
10R10	0.685(0.031)	0.704(0.006)	0.702(0.03)	26.51(0)	26.86(0.2)	312.78(2.87)
30R10	0.601(0.045)	0.692(0.141)	0.681(0.133)	11.97(0)	12.13(0.14)	245.11(3.84)
5R30	0.483(0.034)	0.484(0.018)	0.505(0.022)	60.03(0)	60.14(0.3)	295.11(5.75)
10R30	0.504(0.025)	0.482(0.032)	0.468(0.021)	21.01(0)	20.76(0.09)	236.88(7.87)
30R30	0.448(0.06)	0.411(0.033)	0.392(0.006)	10.93(0)	11.24(0.49)	191.89(8.11)
88R30	0.447(0.036)	0.417(0.025)	0.405(0.023)	1.68(0.001)	2.11(0.12)	61.8(20)
5R50	0.333(0.022)	0.324(0.032)	0.329(0.018)	39.14(0)	39.31(0.3)	190.4(4.5)
10R50	0.18(0.018)	0.224(0.03)	0.225(0.031)	16.3(0.22)	15.96(0)	231.3(12.7)
30R50	0.285(0.012)	0.249(0.009)	0.274(0.023)	10(0.07)	9.83(0.21)	143.66(27.82)
50R50	0.222(0.01)	0.25(0.007)	0.24(0.007)	160.7(5.64)	6.06(0.081)	6.18(0)
30R75	0.17(0.002)	0.12(0.009)	0.13(0.007)	5.37(0)	5.04(0.149)	64.08(12.902)
50R75	0.15(0.017)	0.13(0.004)	0.11(0.008)	5.27(0)	5.13(0.083)	47.79(9.799)
50R100	0.22(0.03)	0.11(0.02)	0.1(0.01)	3.74(0)	2.79(0.11)	7.75
88R100	0142(0.024)	0.067(0.01)	0.05(0.001)	2.26(0)	1.16(0.14)	7.3(1.9)
100R100	0.18(0.03)	0.1(0.01)	0.09(0.02)	2.5(0)	1.64(0.08)	8.69(0.37)

Table 5: Summary of major element glass compositions determined by electron microprobe analysis

	Concentrations (wt%)										
Experiment ID	SiO2	TiO2	Al2O3	FeO	MgO	CaO	Na2O	MnO	K2O	P2O5	Total
5R0	44.7(0.27)	4.59(0.17)	7.03(0.07)	14.26(0.23)	14.24(0.14)	9.9(0.17)	1.95(0.08)	0.19(0.05)	1.06(0.03)	0.63(0.07)	98.54(0.35)
10R0	45.41(0.22)	4.53(0.18)	7.03(0.07)	14.31(0.25)	14.33(0.16)	9.89(0.12)	1.7(0.05)	0.21(0.02)	0.99(0.04)	0.51(0.04)	98.91(0.17)
30R0	45.98(0.21)	4.64(0.22)	7.02(0.09)	13.98(0.26)	14.44(0.07)	9.88(0.1)	1.6(0.05)	0.18(0.04)	0.88(0.02)	0.39(0.03)	98.99(0.47)
5R10	48.01(0.36)	4.07(0.28)	7.62(0.08)	12.77(0.19)	12.87(0.18)	9.05(0.11)	2.3(0.07)	0.19(0.06)	1.35(0.04)	0.49(0.05)	98.7(0.52)
10R10	48.7(0.16)	4.19(0.15)	7.56(0.1)	12.9(0.21)	12.72(0.08)	9.08(0.11)	1.91(0.06)	0.17(0.05)	1.3(0.04)	0.42(0.03)	98.95(0.36)
30R10	49.1(0.45)	4.18(0.2)	7.6(0.12)	12.58(0.33)	12.8(0.12)	9.08(0.07)	1.84(0.04)	0.2(0.03)	1.19(0.03)	0.3(0.03)	98.88(0.32)
5R30	54.11(0.35)	3.22(0.15)	8.97(0.07)	10.44(0.19)	9.97(0.14)	7.43(0.15)	2.49(0.08)	0.14(0.06)	1.95(0.05)	0.47(0.05)	99.19(0.64)
10R30	54.87(0.31)	3.21(0.18)	8.88(0.08)	10.3(0.15)	9.9(0.09)	7.29(0.13)	2.34(0.05)	0.15(0.03)	1.89(0.05)	0.33(0.03)	99.16(0.43)
30R30	54.93(0.29)	3.26(0.17)	8.97(0.11)	9.98(0.15)	10.05(0.09)	7.4(0.12)	2.33(0.08)	0.12(0.04)	1.79(0.04)	0.22(0.03)	99.05(0.42)
88R30	56.35(0.28)	3.7(0.29)	9.26(0.12)	8.08(0.31)	11.75(0.21)	8.46(0.15)	1.03(0.03)	0.13(0.05)	1.08(0.04)	0.1(0.04)	99.93(0.53)
5R50	60.37(0.25)	2.33(0.13)	10.07(0.09)	7.86(0.18)	7.05(0.06)	5.6(0.08)	2.84(0.07)	0.11(0.04)	2.5(0.05)	0.32(0.04)	99.05(0.33)
10R50	60.68(0.32)	2.4(0.23)	10.32(0.16)	7.85(0.19)	7.13(0.14)	5.69(0.13)	2.6(0.13)	0.13(0.06)	2.27(0.09)	-	99.06(0.38)
30R50	61(0.24)	2.34(0.15)	10.23(0.08)	7.42(0.16)	7.24(0.1)	5.69(0.08)	2.66(0.05)	0.13(0.03)	2.46(0.05)	0.16(0.03)	99.32(0.35)
50R50*	-	-	-	-	-	-	-	-	-	-	-
30R75	68.84(0.33)	1.26(0.12)	12.19(0.17)	3.99(0.15)	3.73(0.12)	3.42(0.1)	2.98(0.05)	0.07(0.04)	3.2(0.04)	0.1(0.05)	99.78(0.46)
50R75	69.47(0.43)	1.28(0.11)	12.26(0.14)	4.01(0.26)	3.71(0.09)	3.48(0.09)	2.84(0.09)	0.1(0.05)	2.98(0.1)	0.09(0.04)	100.22(0.63)
50R100*	-	-	-	-	-	-	-	-	-	-	-
88R100	77.24(0.32)	0.21(0.11)	13.95(0.16)	1.08(0.18)	0.27(0.04)	1.31(0.05)	3.3(0.08)	0.05(0.05)	3.62(0.11)	0.08(0.03)	101.09(0.25)
100R100	76.17(0.35)	0.2(0.11)	13.76(0.2)	1.36(0.17)	0.27(0.03)	1.34(0.07)	3.37(0.09)	0.06(0.04)	3.65(0.09)	0.07(0.04)	100.26(0.49)

*Data unable to gather at time of writing this paper. Values assumed based on analyses of similar compositions.

Results

Equilibrium

Equilibrium between PGE and silicate melt appears to have been reached after runs as short as 5hrs. Figure 3 shows Pt and Rh concentrations at all run durations, and the abundances remain relatively constant for a given glass composition. For all analysis, Pt195 was used, as the values are sufficiently similar to Pt194 to illustrate its behavior.

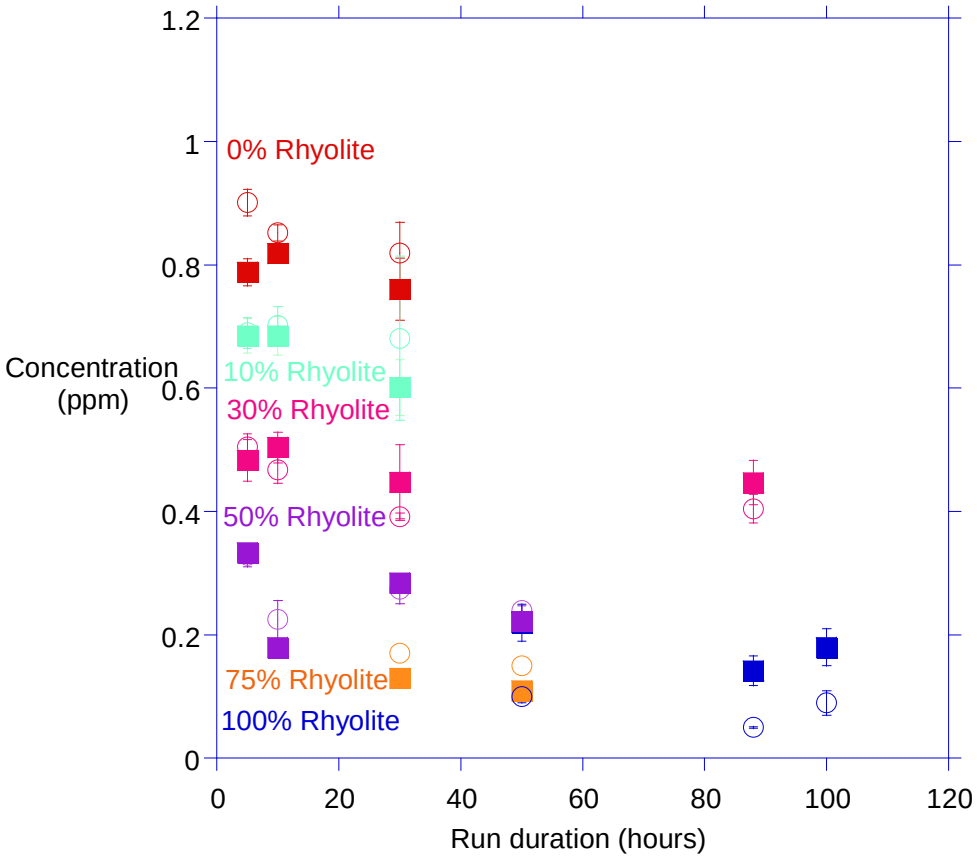

Figure 3: PGE abundance gathered using LA-ICP-MS. Rh103 (square) and Pt195(circle) of each composition are shown here to have similar abundances at all run durations, suggesting that equilibrium is reached as soon as 5hrs into a run.

Solubility as a function of composition

Generally, the solubilities of Pt and Rh were found to decrease as compositions became more rhyolitic (Table 4). A small increase in Rh content between the 75% and 100% rhyolite for the 50 and 100hr runs was observed, but was not necessarily representative of any trend. Results are plotted in Figure 4, showing comparisons between the Pt/Rh concentrations, and the weight percent of common oxides found in basalt and rhyolite. A second degree polynomial trend is seen between these elements and the PGE solubility. The concave nature of this solubility curve is relevant to causing oversaturation of PGE. Had there been a linear relationship observed, as PGE-rich compositions (basalt) were mixed with PGE-free compositions (rhyolite), there would simply be dilution of the PGE. In this situation, concentration would always be below the solubility curve. Figure 4, however, shows that solubility lies below the straight mixing curve and enables the possibility of oversaturation, and therefore precipitation.

To asses this trend in terms of structural differences between felsic and mafic compositions, the NBO/T (non-bridging oxygen per tetrahedrally co-ordinated cation) value was determined for each of the compositions. The NBO/T number is an assessment of the polymerization of a silicate melt, and therefore the availability of bonding sites. The polymerization of silicate melts do not simply depend upon extending chains, but more accurately, they depend on structural units whose proportions change systemically with bulk composition, which is renders NBO/T a more accurate parameter to look at then simply a particular oxide (Mysen, 1986). The calculation method used was that suggested by Mysen (1986). The moles of the cations in the bulk composition are determined and normalized based on the number of oxygens. The Al^{3+} and Fe^{3+} require certain quantities of alkali

metals/earths for charge balance, so these are removed from the total cation sum. The network-modifying cations (Fe(II), Mn, Mg, Na, K, Ca) are summed and divided by the network-forming cations (Si, Ti, Al, Fe(III), and P). Values of NBO/T range from 0 to 4, with pure SiO_2 being 0, and the values determined are consistent with the literature.

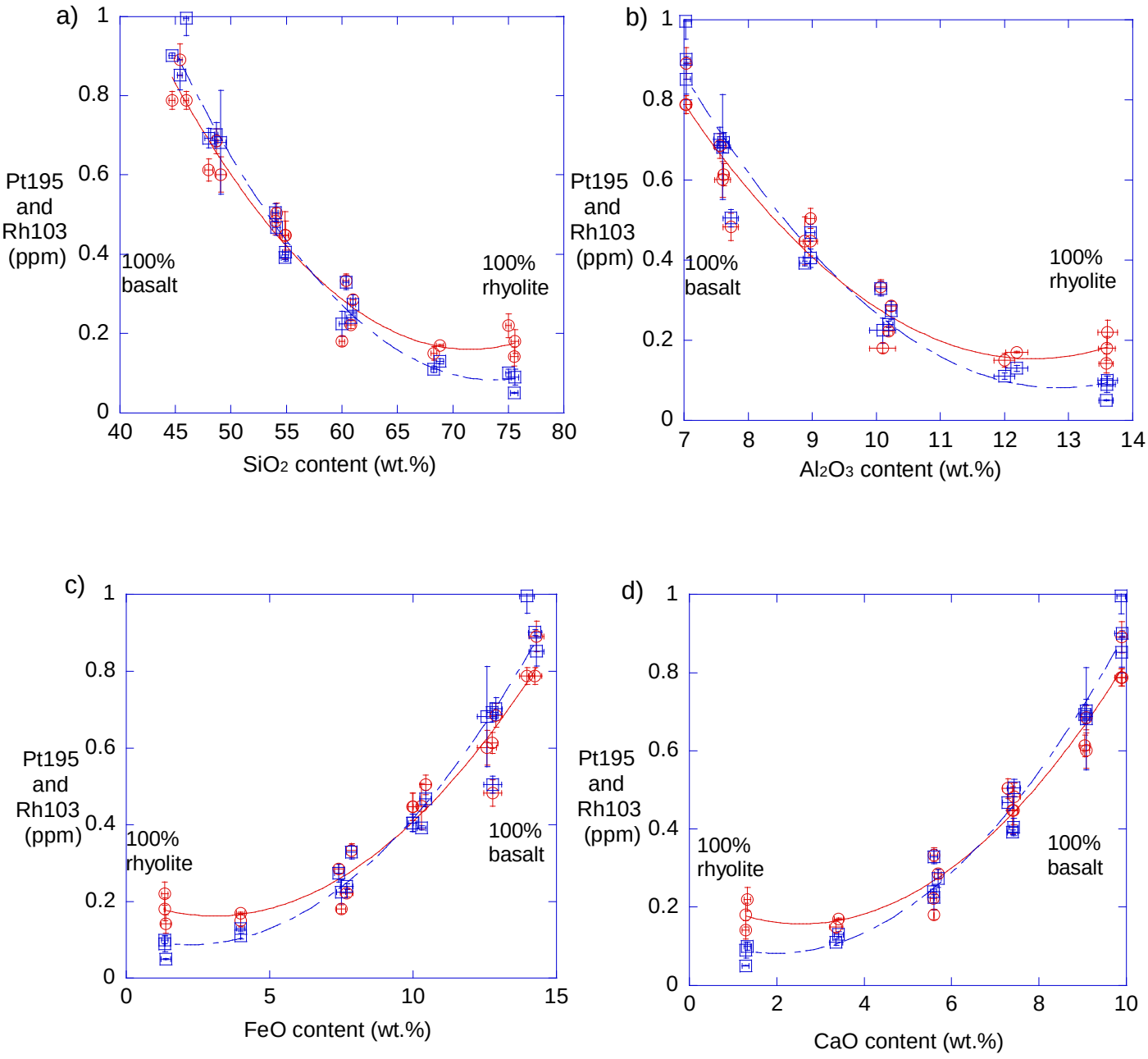

Figure 4: Comparisons of Pt195 (blue squares) and Rh103 (red circles) concentrations to a)SiO_2 content; b) Al_2O_3 content; c) FeO content; and d) CaO content in glasses. A second order polynomial was fit to the data, showing trends relating to silicate melt compositions, with rhyolite having higher Al_2O_3 and SiO_2 and basalt having higher FeO and CaO.

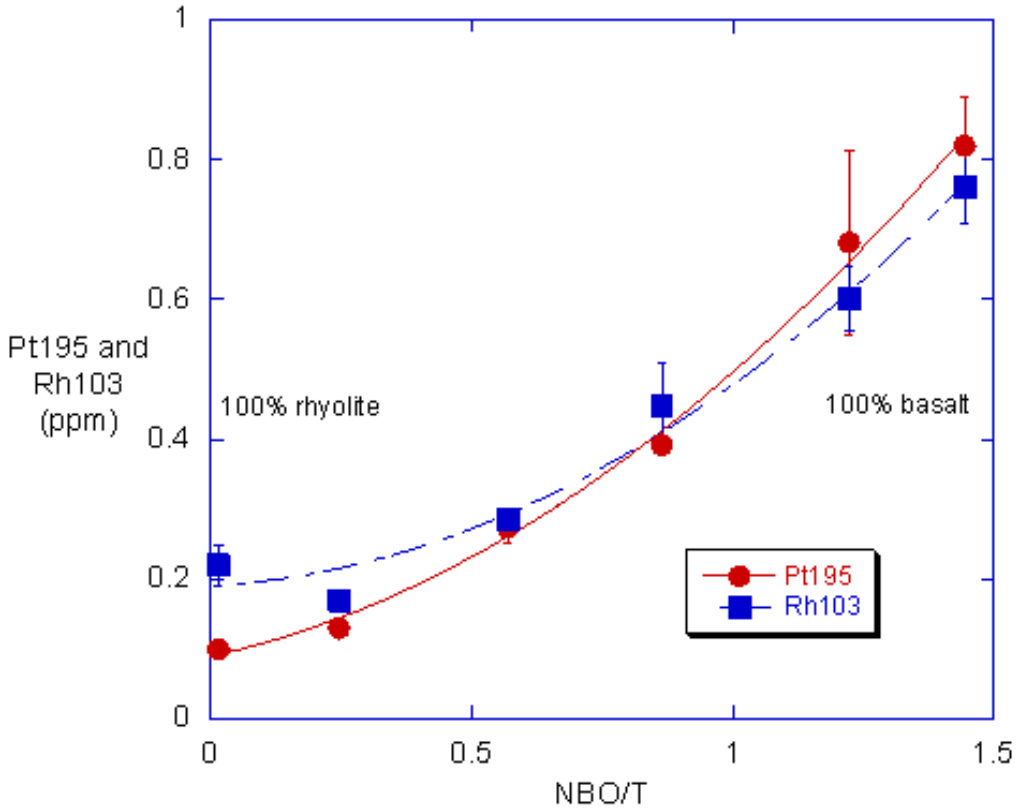

Figure 5: Concentrations of Rh103 (blue squares) and Pt195 (red circles) in ppm as a function of NBO/T for selected run durations (≥30hrs).

Discussion

Structural control of PGE dissolution

The observed decrease in PGE solubility as a function of increasing rhyolite content in silicate melt compositions is a possible response to the degree of polymerization (Figure 5). When Pt195 and Rh103 are exposed to oxidizing conditions, as was done in the experiments completed for this paper, they form metal oxides. Previous work suggests that Rh2+ is the dominant oxidation state except at very high fO_2, and Pt2+ and Pt4+ are typical for moderately oxidizing conditions (Ertel *et al.*, 1999).

According to Mysen (1986), silicate melts behave in a way determined by their structural coordination. Bridging oxygen (BO) surrounding the central, tetrahedrally-coordinated cation link tetrahedra, and other oxygen atoms link the tetrahedral cation to metal cations (NBO). The metals are the network modifiers, and the type of metal cation is relevant to how disruption of the silicate melt occurs. Fargus *et al.* (1999) go on to say that Pt (specifically $Pt^{4+}O_6$) may show preferential connection to network modifiers above network formers, and must bond to non-bridging oxygen. Pt is known to prefer square planar configurations, and in the case of $Pt^{4+}O_6$, the octahedral configuration is not easily incorporated into tetrahedral networks. With fewer preferred bonding sites available, it is suspected that Pt will not readily dissolve into SiO_2-rich melts.

The asymptotic nature of the curve suggests that there is something other than NBO/T controlling the solubility. Farges *et al.* (1999) suggest that another means to dissolve Pt^{4+} in a melt may include charge balancing from Ca^{6+}, in addition to either Si^{4+} or $Al^{4+/5+}$.

Regarding Al_2O_3, the results appear to contradict those of Farges, *et al.* (1999), who suggested that the presence of Al_2O_3 increases the dissolution of Pt in the CAS-system, contrary to the effect of SiO_2. However, since the observation was made only as a comparison to SiO_2, it probably suggests that Al_2O_3, as a 3+ species requiring further charge balance, has a significantly smaller contribution to inhibiting Pt dissolution than does SiO_2. The apparent relationship seen in Figure 4b may exist simply as a consequence of the stronger control by SiO_2 on the system, and it is unadvisable to assume that oxides other than silica in Figure 4 perform important structural coordination functions.

The overall similarity in dissolved PGE concentration is interesting in itself, as the alloy used had a 9:1 ratio of Pt to Rh. Rhodium must therefore be more soluble than Pt, as its activity in this system is 4 times less than that of Pt. The observation was reinforced through the 100% rhyolite runs, where analyses showed heterogeneity in Pt, and homogeneity in Rh, suggesting that only Pt had precipitated (Figure 6). All previously examined micronuggets (for compositions between 0-75% rhyolite in basalt) had shown similar behavior for Rh and Pt. The discrepancy in the solubility behavior of the PGEs can be looked at in terms of thermodynamic and structural (as mentioned above) properties. According to Palme (2008), Pt has the least stable oxide of all the Pt group elements. The stability ranking is based on reduction potentials of PGE oxides. Of the PGE, P-PtO_2 has the highest reduction potential and RuO_2 has the lowest, with Rh_2O_3 being almost exactly between the two. The dissolution of Pt requires greater energy than does the dissolution of Rh.

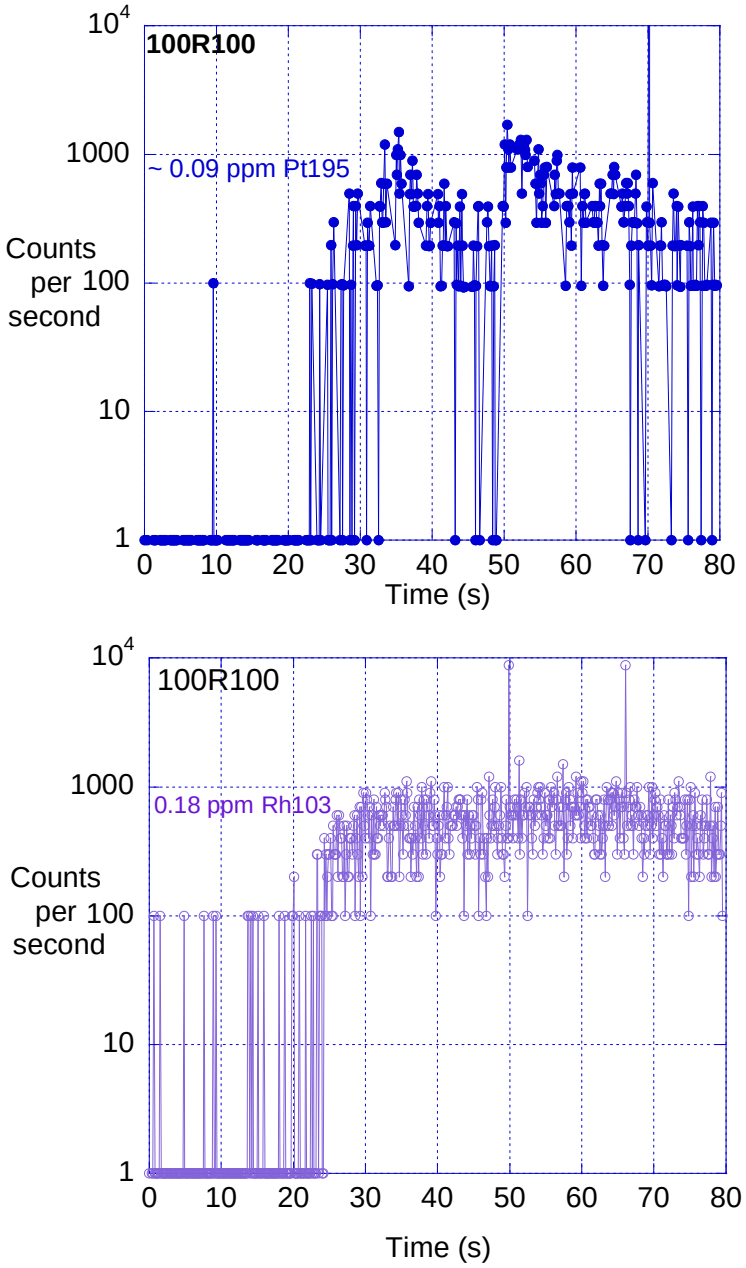

Figure 6: Comparison of Pt heterogeneity and Rh homogeneity for the same ablation line, as determined by LA-ICP-MS. The sample comprises 100% rhyolite, and was run for 100 hrs.

Oversaturation model

For PGE to precipitate from a melt and ascertain itself as insoluble, it must be oversaturated in the melt. A model is for whether oversaturation has occurred can be determined by examining diffusion within the melt and calculating the time-evolution curve. Diffusion is important, as it is the rate limiting process at the interface between 2 phases.

The steady-state flux of matter across a plane is given by Fick's 1st law

$$J_x = -D(dc/dx), \qquad (9)$$

where J_x (units of mass/L^2t) is the flux, D (L^2/t) is the diffusion coefficient, x (L) is the distance matter has diffused, and c (mass/L^3) is the concentration of the compound of interest. In the case where concentration is changing at positions with time and steady state does not exist, the form of the equation

$$dc/dt = -d/dx(Ddc/dx) \qquad (10)$$

can be used. In this case the silica diffusion profile was generated as it is the slowest moving, and therefore the rate limiting compound within the melt compositions. The profile is calculated based on the pure rhyolite and pure basalt being a pair of semi-infinite solids whose initial concentrations create a step function when plotted as concentration vs. distance. In this case, where the SiO_2 initial concentration is not zero, boundary conditions are determined and the equation

$$c(x,t) - c_0 = (c' - c_0)/2*[1 - erf(x/2*\sqrt{D}t)] \qquad (11)$$

is used, where c_0 is the initial concentration, c' is the final (or other initial) concentration, and c(x,t) is the concentration at a given position and time (Shewmon, 1983).

The boundary conditions chosen for the calculation of the diffusion profile were 75.5% SiO_2 for rhyolite and 45% SiO_2 for basalt. A *D* value for SiO_2 was estimated from Watson (1982) to be 10^{-7} at 1400°C. The Pt and Rh solubilities were determined for each SiO_2 content using the curves in Figure 4a (Pt/Rh (ppm) vs. SiO_2 (wt.%)), which yielded the equations:

$$Pt(SiO_2) = 4.9726 - 0.134x + 0.0009x^2 \quad (13)$$

$$Rh(SiO_2) = 5.08 - 0.1337x + 0.00089x^2. \quad (14)$$

Plotting PGE concentration and solubility as a function of diffusion distance (Figures 7, 8), shows the measurable difference between the two quantities. When the concentration is greater than the solubility, precipitation can occur within a melt. This process also occurs as a function of time. For interdiffusion events of 5 hrs (Figures 7a, 8a), there is a significant physical zone of undersaturation visible, but for events of 20 hrs (Figures 7b, 8b), the undersaturated areas only occur at the very extremes of the system, and tend to show a greater difference in concentration and solubility.

An experiment which could demonstrate this effect might include Pt (or Rh) saturated basalt sitting adjacent to Pt-free rhylolite, and being heated for enough hours to create adequately large zones of oversaturation and undersaturation (perhaps ~4hrs). The interface between the two phases (x = 0) should show precipitation of the PGE. The

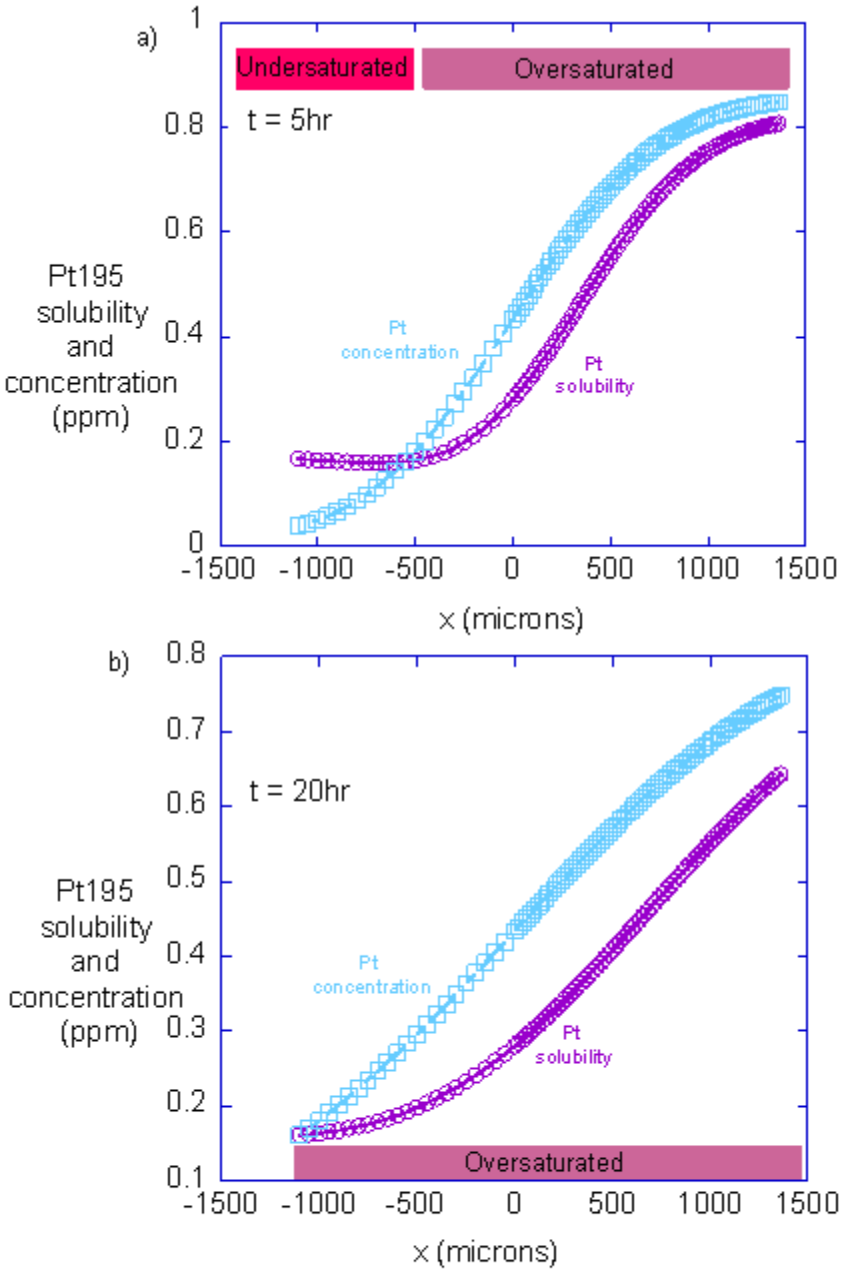

Figure 7: Solubility and concentration of Pt are shown along silica diffusion profile at ~1400C. Image a) shows diffusion after 5hrs, and b) shows diffusion after 20hrs. When Pt concentration is greater than Pt solubility, oversaturation in silicate melt occurs.

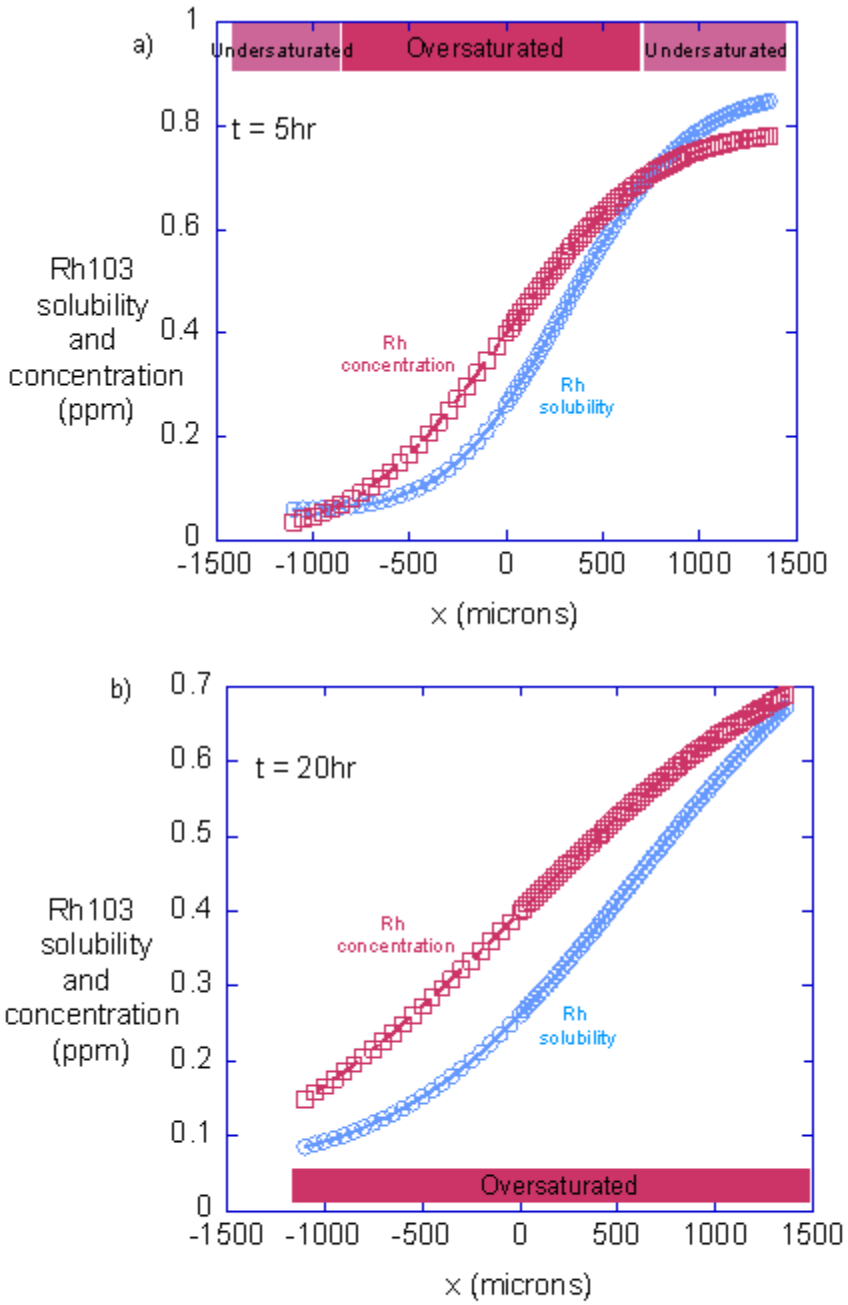

Figure 8: Solubility and concentration of Rh are shown along silica diffusion profile at ~1400C. Image a) shows diffusion after 5hrs, and b) shows diffusion after 20hrs. When Rh concentration is greater than Rh solubility, oversaturation in silicate melt occurs.

foreseeable problem is that the degree of oversaturation (~0.1 ppm) may not be large enough to overcome surface energy and nucleate. Perhaps the addition of nuclei prior to melting will be necessary to observe precipitation in this system.

Conclusion

A compositional dependence was established for the solubility of Pt and Rh. The partition coefficients of the Pt and Rh in this series of systems are scaled to the change in concentration across the compositional range. Changes of ~1 order of magnitude are observed in this experiment, suggesting that for this portion of the ultra-mafic – felsic spectrum, compositional dependence is small, particularly compared to fO_2 dependence (Ertel *et al.* 1999). Temperature dependence, as tested by Fortenfant *et al.* (2003) also showed changes within 1 order of magnitude, but only for a limited temperature range (~250°C).

For researchers conducting experiments on PGE parameters, the data presented above could be relevant. For example, previous studies (Ertel, *et al.*, 1999; Fortenfant *et al.*, 2002) have been conducted at the diopside-anorthite eutectic composition, which has an NBO/T = 0.5. Experimental conditions could be improved by selecting a composition which promotes PGE dissolution.

In addition, the concentration of PGE in chromatites could be illuminated by this study. As chromite is thought to crystallize by means of magma mixing, PGE may also precipitate due to the addition of felsic crustal materials. If the magmas are already saturated in PGE, then perhaps the change in composition, along with the addition of chromite nuclei, is all that is required to 'tip the scale', and cause PGE precipitation (Irvine, 1975).

Further studies on PGE across the mafic to ultra-mafic compositional spectrum are required to generate a robust data set and thorough understanding of the compositional dependence of PGE solubility.

References

Best, M. G. (1982). *Igneous and Metamorphic Petrology*. New York: W. H. Freeman and Company.

Borisov, H. (2008). Platinum-group elements in cosmochemistry. *Elements, 4* 233-238.

Borisov, A.., Palme, H. (1997). Experimental determination of the solubility of platinum in silicate melts. *Geochimica et Cosmochimica Acta, 61* 4349-4357.

Borisov, A., Palme, H. (2000). Solubilities of noble metals in Fe-containing silicate melts as derived from experiments in Fe-free systems. *American Mineralogist, 85* 1665–1673.

Borisov A., Palme, H., Spettel, B. (1994). Solubility of palladium in silicate melts: Implications for core formation in the Earth. *Geochimica et Cosmochimica Acta, 58* 705-716.

Ertel, W., Dingwell, D.B, Sylvester, P.J. (2008). Siderophile elements in silicate melts — A review of the mechanically assisted equilibration technique and the nanonugget issue. *Chemical Geology, 248* 119-139.

Ertel, W., O'Neill, H. St. C., Sylvester, P. J., Dingwell, D. B. (1999). Solubilities of Pt and Rh in a haplobasaltic silicate melt at 1300°C. *Geochimica et Cosmochimica Acta, 63* 2439-2449.

Fargus, F., Neuville, D. R., Brown, G. E. JR. (1999). Structural investigation of platinum solubility in silicate glasses. *American Minerologist*, *84* 1562-1568.

Fortenfant, S. S., Gunther, D., Dingwell, D. B., Rubie, D. C. (2003). Temperature dependance of Pt and Rh solubilities in a haplobastaltic melt. *Geochimica and Cosmochimica Acta, 67* 123-131.

Hogg-Cowper, A. J. C. (1985). The petrology and geochemistry of the Prisen af Wales Bjerge, east Greenland [Master's thesis]: University of Toronto.

Holzheid, A.., Sylvester, P., O'Neill, H. St C., Rubie, D. C., & Palme, H. (2000). Evidence for a late chondritic veneer in the Earth's mantle from high-pressure partitioning of palladium and platinum. *Nature, 406* 396-399.

Irvine, T.N. (1975). Crystallization sequences in the Muscox intrusion and other layered intrusions-II. Origins of chromatite layers and similar deposits of other magmatic ores. *Geochimica and Cosmochimica Acta, 39* 991-1020.

Mysen, B.O. (1986). Structure and petrologically important properties of silicate melts relevant to natural magmatic liquids. In C.M. Scarfe (Ed.), *Short Course in Silicate Melts* (pp. 180-209). Ottawa, ON: Mineralogical Association of Canada.

Righter, K., Campbell, A.J., Humayun, M., Hervig, R.L. (2004). Partitioning of Ru, Rh, Pd, Re, Ir, and Au between Cr-bearing spinel, olivine, pyroxene and silicate melts. *Geochimica et Cosmochimica Acta, 68* 867–880.

Ryerson, F.J., Watson, E.B. (1987). Rutile Saturation in magmas: implications for Ti-Nb-Ta depletion in island-arc basalts. *Earth and Planetary Science Letters 86* 225-239.

Shewmon, P.G. (1983). Diffusion in Solids. Jenks OK.: J. Williams Book Co.

Walter M. J., Thibault, Y. (1995). Partitioning of tungsten and molybdenum between metallic liquid and silicate melt. *Science, 270* 1186-1189.

Watson, B. (1982). Basalt contamination by continental crust: some experiments and models. *Contributions to Mineralogy and Petrology 80* 73-87.